ACS APPLIED MATERIALS & INTERFACES

Research Article

www.acsami.org

A Systematic Study on the Influence of Electron-Acceptors in Phenanthrocarbazole Dye-Sensitized Solar Cells

Lin Yang,[†,§] Zhaoyang Yao,[†,§] Jiao Liu,[†,§] Junting Wang,[†,§] and Peng Wang*[,†,‡]

[†]State Key Laboratory of Polymer Physics and Chemistry, Changchun Institute of Applied Chemistry, Chinese Academy of Sciences, Changchun 130022, China

[‡]Department of Chemistry, Zhejiang University, Hangzhou 310028, China

[§]University of Chinese Academy of Sciences, Beijing 100049, China

Supporting Information

ABSTRACT: In this work, by conjugating 2-cyanoacrylic acid (CA), 4-(benzo[*c*][1,2,5]thiadiazol-7-yl)benzoic acid (BTBA), 4-(7-ethynylbenzo[*c*][1,2,5]thiadiazol-4-yl)benzoic acid (EBTBA), and 4-((7-ethynylbenzo[*c*][1,2,5]thiadiazol-4-yl)-ethynyl)benzoic acid (EBTEBA) to a binary electron-donor diphenylamine-phenanthrocarbazole (DPA-PC), we systematically investigate the impacts of electron-acceptors upon energy level, energy gap, light-harvesting ability, photovoltaic parameter, and cell stability of donor−acceptor dyes in photoelectrochemical cells. In conjunction with an ionic liquid composite electrolyte, the DPA-PC dye with EBTEBA as electron-acceptor yields a high power conversion efficiency of 8% and an outstanding stability after a 1000 h aging test under the soaking of full sunlight at 60 °C in a dye-sensitized solar cell. Femtosecond fluorescence up-conversion measurements have suggested that energy relaxation and electron injection both occur to dye molecules in the nonequilibrium excited states. Moreover, the time constants of injecting electrons from dye molecules in the excited states to titania are very dispersive for over 1 order of magnitude, mainly owing to the broad energy distribution of excited states.

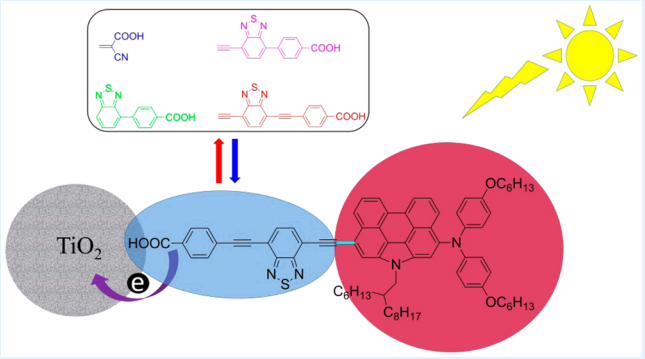

KEYWORDS: *solar cell, perylene, ultrafast spectroscopy, excited state, charge transfer*

1. INTRODUCTION

Dye-sensitized solar cell (DSC) technology has received considerable attention from researchers owing to its distinctive trait of using less hazardous and less energy-intensive materials for manufacture,[1] until the recent surging investigations on the lead-based perovskite solar cell with high PCEs under an irradiance of 100 mW cm^{-2}, air mass global (AM1.5G) sunlight.[2] Meanwhile, a Japanese team demonstrated a DSC with a marvelous PCE of 14.5% in 2015,[3] incarnating an over 10 years expedition on organic dyes,[4−10] one-electron redox couples,[11−18] and molecular-scale interface engineering.[19−22] To further boost the PCE of a DSC under the AM1.5G conditions, it will be of paramount importance to design low optical gap donor−acceptor (D−A) dyes characteristic of a dual power of harvesting infrared photons and injecting carriers to charge transporter in excellent yields, and at the same time to attenuate charge recombination via modulating the microstructure of self-organized dye-layer. Consequently, some low optical gap organic dyes were reported, but most of them cannot be employed to make DSCs with high external quantum efficiencies (EQEs).[23−26] This circumstance is possibly concerned with the stabilized lowest unoccupied molecular orbital (LUMO) energy levels, destabilized highest occupied molecular orbital (HOMO) energy levels, or even both of those dyes, because the reduction of driving energy could slow down the kinetics of carrier injection.[27−29] Moreover, a low optical gap dye in the excited state may have a shortened lifetime according to the energy gap law.[30] An extremely fast deactivation of excited state via conical intersection may intercept the channel of electron injection remarkably.

The polycyclic aromatic hydrocarbon *N*-annulated perylene (1*H*-phenanthro[1,10,9,8-*cdefg*]carbazole, PC) with a planar electronic skeleton has been used by Luo et al. as an auxiliary electron-releasing block in zinc porphrin dyes for enhanced absorption of infrared solar photons.[31] It can be discerned from Figure S1 that the HOMO energy level (−5.23 eV) of PC is 0.40 eV lower than that (−4.83 eV) of electron-donor triphenylamine-cyclopentadithiophene (TPA-CPDT) used for our model organic dye C218 and C258.[32,33] Thereby in the initial exploration of PC for low optical gap D−A dyes,[34] we constructed a binary electron-donor DPA-PC (Figure 1) with an improved HOMO energy level of −4.83 eV and simply

Received: February 18, 2016
Accepted: March 30, 2016
Published: March 30, 2016

DOI: 10.1021/acsami.6b02075
ACS Appl. Mater. Interfaces 2016, 8, 9839−9848

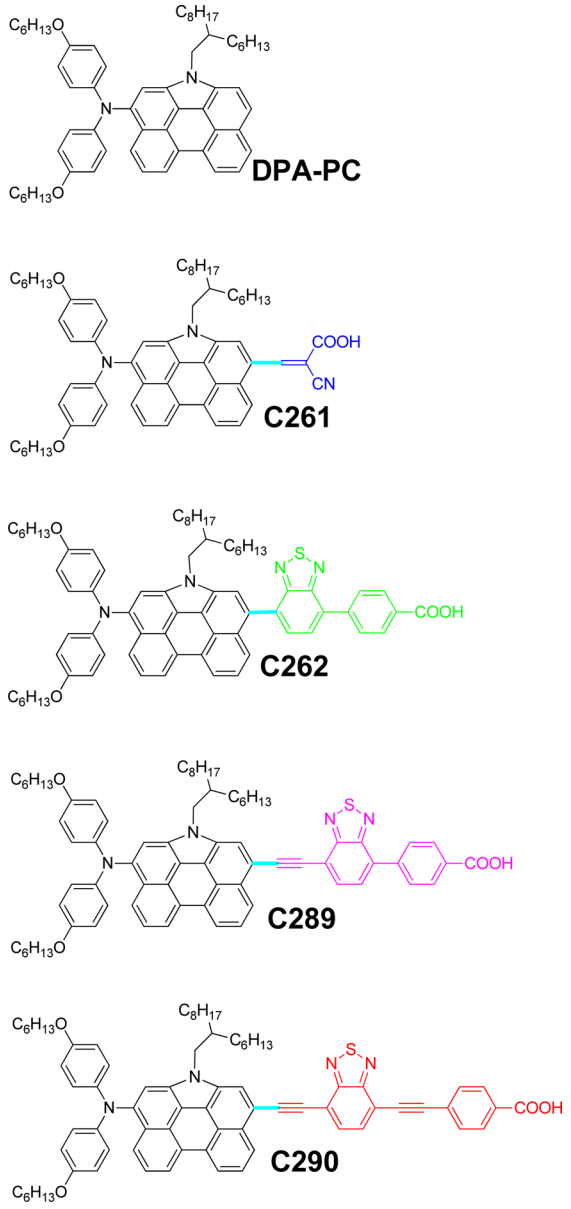

Figure 1. Chemical structures of D−A dyes C261, C262, C289, and C290 characteristic of (blue) CA, (green) BTBA, (magenta) EBTBA, and (red) EBTEBA as the respective electron-acceptors, combined with (black) a binary electron-donor DPA-PC. One can consider that the bond marked with the color of cyan is formed by coupling of electron-rich and electron-deficient entities via oxidative dehydrogenation.

combined it with the conventional electron-acceptor CA for C261. The first metal-free PC dye C261 has a relatively low optical gap and achieved a fairly good PCE of 8.8% in conjunction with a highly volatile cobalt electrolyte. Our subsequent study has shown that dissimilar to the impact of replacing CA with BTBA for dyes C218 and C258 with TPA-CPDT as the electron-donor, dye C262 with DPA-PC and BTBA has a blue-shifted absorption peak and a lower PCE of 7.3% in comparison with C261, owing to the significant twisting between PC and BTBA.[35] Also, there is a large twisting between benzo[*c*][1,2,5]thiadiazole (BT) and benzoic acid (BA). To address these issues, we have resorted to electron-acceptors EBTBA and EBTEBA for other PC-based dyes.[36,37]

Theoretical calculations (Figure S2) disclose that the LUMO energy levels of these four electron-acceptors decline in the order CA > BTBA > EBTBA > EBTEBA, and their HOMO energy levels climb in the order CA < BTBA < EBTBA < EBTEBA. In this paper, we will first execute a systematic analysis on the influences of these electron-acceptors upon the frontier molecular orbital (FMO) energy levels, energy gaps, light absorption of DPA-PC dyes C261, C262, C289, and C290 (Figure 1), on the basis of joint theoretical calculations and experimental measurements. To reveal the occurrence of energy relaxation of excited states of these D−A dyes and the electron injection kinetics from an excited-state dye to the conduction-band (CB) of titania, we further performed static and dynamic photoluminescence (PL) measurements. Furthermore, these dyes grafted on a bilayer titania film will be employed along with an iodine-based ionic liquid composite electrolyte for DSC fabrication. At the end, electrical and photophysical measurements will be performed to scrutinize the origins behind the variation of cell parameters before and after 1000 h aging under the soaking of full sunlight at 60 °C.

2. RESULTS AND DISCUSSION

Cyclic voltammetric measurements of the THF solutions were first performed to disclose the influences of different electron-acceptors upon energy levels and energy gaps of D−A dyes. As illustrated in Figure 2, the HOMO energy levels and LUMO

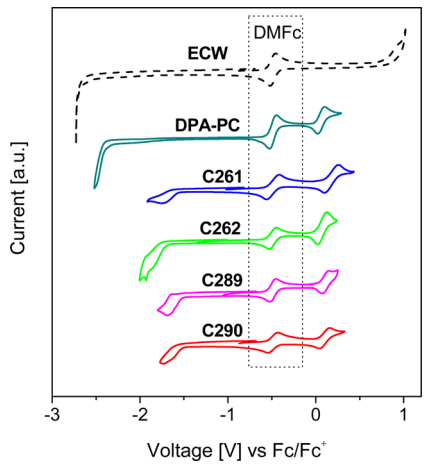

Figure 2. Cyclic voltammograms of DPA-PC, C261, C262, C289, and C290 in THF. 0.1 M of 1-ethyl-3-methylimidazolium bis-(trifluoromethanesulfonyl)imide (EMITFSI) was used as the supporting electrolyte. Electrochemical window (ECW) with a glassy carbon working electrode was also included to show that Faradaic current in solid curves are indeed associated with DPA-PC, C261, C262, C289, and C290. Scan rate: 5 mV s^{-1}. Decamethylferrocene (DMFc) was added as the internal reference and all potentials were further calibrated with the standard redox couple ferrocene/ferrocenium (F_C/F_C^+) as the reference.

energy levels versus vacuum of the four D−A dyes and DPA-PC could be approximately estimated by

$$E = -4.88 - eE_{onset} \quad (1)$$

where E_{onset} is the onset potential of oxidizing or reducing a molecule at the ground-state. The detailed parameters are compiled in Table 1. As illustrated in Figure S3a and S3b, the electrochemically measured FMO energy levels (E_L^{CV} and E_H^{CV}, Table 1) of DPA-PC, C261, C262, C289, and C290 can be

DOI: 10.1021/acsami.6b02075
ACS Appl. Mater. Interfaces 2016, 8, 9839−9848

Table 1. Experimental and Theoretical Data on Energy Levels, Electronic Absorption, and PL of DPA-PC, C261, C262, C289, and C290[a]

dye	E_L^{CV} (eV)	E_L^{B3LYP} (eV)	E_H^{CV} (eV)	E_H^{B3LYP} (eV)	$\Delta E_{L/H}^{CV}$ (eV)	$\Delta E_{L/H}^{B3LYP}$ (eV)	$\lambda_{ABS\ MAX}^{MEAS}$ (nm)	$\lambda_{ABS\ MAX}^{TD\text{-}MPW1K}$ (nm)	$\lambda_{PL\ MAX}^{MEAS}$ (nm)	$\lambda_{PL\ MAX}^{TD\text{-}MPW1K}$ (nm)	$\Delta\bar{\nu}^{MEAS}$ (10^3 cm^{-1})
DPA-PC	−2.48	−2.01	−4.87	−4.83	2.39	2.82	467	433	533	510	2.7
C261	−3.31	−2.88	−5.00	−5.04	1.69	2.16	573	541	666	601	2.4
C262	−3.19	−2.75	−4.87	−4.84	1.68	2.09	489	522	690	652	6.0
C289	−3.32	−2.94	−4.90	−4.86	1.58	1.92	550	560	691	653	3.7
C290	−3.35	−3.10	−4.91	−4.87	1.56	1.77	569	596	704	679	3.4

[a]Energy levels of LUMO and HOMO (E_L^{CV} and E_H^{CV}) versus vacuum and frontier orbital energy gap ($\Delta E_{L/H}^{CV}$) were estimated from CVs displayed in Figure 2. H and L denote HOMO and LUMO. LUMO and HOMO (E_L^{B3LYP} and E_H^{B3LYP}) energy levels and energy gap ($\Delta E_{L/H}^{B3LYP}$) were calculated at the B3LYP/6-311G(d,p) level of theory for a dye molecule in THF. Maximum absorption wavelength ($\lambda_{ABS\ MAX}^{MEAS}$), maximum PL wavelength ($\lambda_{PL\ MAX}^{MEAS}$), and Stokes shift ($\Delta\bar{\nu}^{MEAS}$) were inferred from electronic absorption and PL spectroscopies of toluene solutions presented in Figure 4. Maximum absorption wavelength ($\lambda_{ABS\ MAX}^{TD\text{-}MPW1K}$) and maximum PL wavelength ($\lambda_{PL\ MAX}^{TD\text{-}MPW1K}$) were calculated at the TD-MPW1*K*/6-311G(d,p) level of theory for a dye molecule in toluene.

primely correlated with those based on the DFT calculations at the B3LYP/6-311G(d,p) level (E_L^{B3LYP} and E_H^{B3LYP}, Table 1). As presented in Figure 3a, we also analyzed the HOMO energy

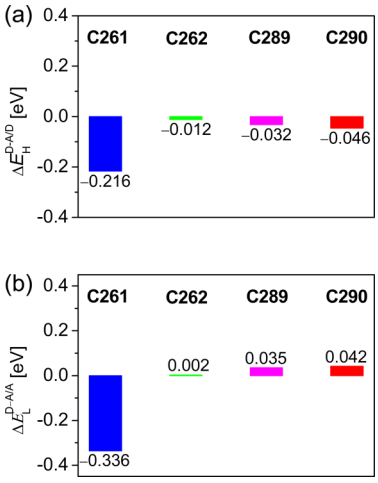

Figure 3. (a) The HOMO energy level difference between a D−A dye (C261, C262, C289, or C290) and an electron-donor (DPA-PC), $\Delta E_H^{D-A/D}$, which is defined as $E_H^{D-A} - E_H^{D}$. The $\Delta E_H^{D-A/D}$ value signifies the extent to which attaching an electron-acceptor to an electron-donor affects the HOMO energy level. (b) The LUMO energy level difference between a D−A dye (C261, C262, C289, or C290) and an electron-acceptor (CA, BTBA, EBTBA, or EBTEBA), $\Delta E_L^{D-A/A}$, which is defined as $E_L^{D-A} - E_L^{A}$. The $\Delta E_L^{D-A/A}$ value signifies the extent to which attaching an electron-donor to an electron-acceptor affects the LUMO energy level.

level difference ($\Delta E_H^{D-A/D}$) of a D−A dye with respect to electron-donor DPA-PC. It turns out that the attachment of electron-acceptors has in general brought forth a HOMO stabilization, the extent to which varies in the order CA ≫ EBTEBA > EBTBA > BTBA. Further analysis of the LUMO energy level difference ($\Delta E_L^{D-A/L}$) of a D−A dye with reference to its electron-acceptor does not give a consistent conclusion (Figure 3b). While C261 owns a remarkably stabilized LUMO energy level with respect to CA, the other three dyes (C262, C289, and C290) all possess slightly destabilized LUMO energy levels against their respective electron-acceptors (BTBA, EBTBA, and EBTEBA). Obviously, the LUMO energy levels of these dyes (C262, C289, and C290) align in the same tendency as those of their electron-acceptors, except for C261 with CA as the electron-acceptor. At the moment, we still do not have a very clear clue on the stabilization of HOMO/LUMO to a larger extent for dyes using CA as the electron-acceptor. In general, it should be related to the distribution profile of frontier molecular orbitals. On the basis of these analyses, in stark contrast to the counterpart with the conventional electron-acceptor CA, one could anticipate that the usage of a new generation electron-acceptor such as BTBA, EBTBA, and EBTEBA should endow a D−A dye with FMO energy levels closely inherent from its electron-donor and electron-acceptor. Also, the experimental and theoretical energy gaps ($\Delta E_{L/H}^{CV}$ and $\Delta E_{L/H}^{B3LYP}$, Table 1) of these molecules are well correlative as shown in Figure S3c and narrow in the order of DPA-PC > C261 > C262 > C289 > C290.

Next, we measured the static absorption and PL spectroscopies (Figure 4) of these molecules in toluene. As Figure

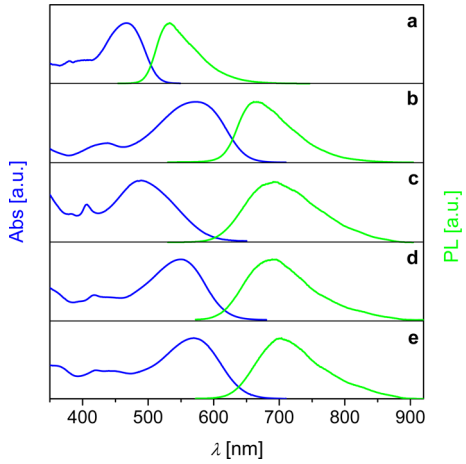

Figure 4. Electronic absorption and photoluminescence spectra of 10 μM of (a) DPA-PC, (b) C261, (c) C262, (d) C289, and (e) C290 in toluene.

S3d,e illustrates, the maximum absorption and PL wavelengths ($\lambda_{ABS\ MAX}^{MEAS}$ and $\lambda_{PL\ MAX}^{MEAS}$, Table 1) are nicely correlated with those from the TDDFT calculations at the MPW1K/6-311G(d,p) level ($\lambda_{ABS\ MAX}^{TD\text{-}MPW1K}$ and $\lambda_{PL\ MAX}^{TD\text{-}MPW1K}$, Table 1). The measured Stokes shifts in Table 1 for these molecules range from 2.4×10^3 cm^{-1} (0.298 eV) to 6.0×10^3 cm^{-1} (0.744 eV). The energy losses are intrisincally related to the vibrational and torsional relaxations of vertically excited states.[38] Herein, by using the TDDFT calculation at the TD-MPW1K/6-311G(d,p) level, the equilibrium geometry in the first excited singlet states (S_1^{eq})

DOI: 10.1021/acsami.6b02075
ACS Appl. Mater. Interfaces 2016, 8, 9839−9848

was optimized to investigate torsional relaxation. Moreover, in terms of the Franck−Condon (FC) principle, the geometry in the vertically excited first singlet state (S_1^{vert}) inheritates that of S_0. Consequently, resorting to the optimized geometries of S_0 and S_1^{eq}, conformational changes in the excited states could be discerned. Sizable variations in the triarylamine moiety can be identified from Figure S4. The S_1^{eq} of dyes C262 and C289 display more planar electronic backbones.

The time-resolved PL traces of DPA-PC, C261, C262, C289, and C290 in toluene (Figure S5−S9) were also recorded by joint use of the time-correlated single-photon counting and femtosecond fluorescence up-conversion techniques. We have found that each PL curve is not dependent on the wavelength and intensity of excitation lights. Clearly all molecules exhibit PL wavelength dependent kinetics. Fast decays at the high-energy PL wavelengths are concomitant with slow arising signals at the low-energy PL wavelengths. By use of the free Glotaran software,[39] PL curves for each molecule were globally fitted with four time constants (τ_i), which were collected in Table S1−S5. Note that to get a satisfactory global fitting, at least four time constants were needed for all samples. On the basis of time constants derived from global fittings, a four-exponential function convoluted with a Gaussian instrument response function were employed to yield the corresponding fractional amplitudes (A_i, Table S1−S5) by using the Surface Xplorer software (version 2.3). The average lifetimes ($\bar{\tau}$, Table S1−S5) were calculated by use of equation

$$\bar{\tau} = \sum_{i=1}^{n} A_i \tau_i / \sum_{i=1}^{n} A_i \quad (2)$$

where $A_i > 0$. It is evident from Figure S10 that there is a gradual increase of $\bar{\tau}$ for every molecule along with the red-shifting of PL wavelength, up to 3 orders of magnitude. Recalling that the integral of dynamic PL trace at a certain wavelength (Figure S5−S9) is eventually propotional to the counts of emiting photons at a corresponding wavelength in the stationary PL spectra (Figure 4), we reconstructed time-resolved emission spectra (TRES) as shown in panels a−e of Figure S11, and derived evolution associated emission spectra (EAES) as presented in panels f−j of Figure S11 by use of the Glotaran software. Dynamic Stokes shifts ocuur to all molecules studied here. We do not consider that this behavior is related to the emission of excimers formed by aggregation, because 10 times dilution of solutions only results in weak PL signals but does not alter normalized PL traces at all. Actually, this scenario could be depicted by a picture that upon light excitation, the dye molecules go through intramolecular charge transfer to form the S_1^{vert} within 1 fs. The S_1^{vert} possesses the same geometry as the S_0, but undergoes vibrational relaxations within ∼100 fs and stepwise torsional relaxations within longer time delays to form S_1^{eq}.[40−45] According to the considerable conformational variations of S_0 and S_1^{eq} (Figure S4), the occurrence of torsional relaxations is highly conceivable.

To roughly assess if the stepwise adjustment of electron-acceptors in D−A dyes will impact the yield of injecting electrons from the electronically excited state to titania, ϕ_{ei}, we employed a high-sensitivity ICCD camera in conjunction with a cw laser diode as the excitation resource to record stationary PL spectroscopies of dye-adsorbed alumina and titania films. We further derived the quenching yield of steady-state PL at a series of wavelengths, QY^S, by use of equation

$$QY^S(\lambda) = 1 - \frac{I_{PL}(T, \lambda)}{I_{PL}(A, \lambda)} \quad (3)$$

where I_{PL} (A, λ) and I_{PL} (T, λ) denote the wavelength dependent PL counts for dyes on alumina and titania, respectively. A dye at the high-energy excited state carries a large free energy and thereby emits a photon at the short wavelength, and vice versa. As presented in Figure 5a, the high-energy excited state of each dye exhibits a much lower QY^S than its cooled excited state. So far this phenomenon has been rarely remarked in the literatures on DSCs. To gain more insights, we also exposed the dyed oxide films to fs pulse excitation and recorded the time-resolved traces (Figures S12−S15 and S18−S21) at a variety of PL wavelengths. We have found that all dyes self-organized on the surface of alumina and titania nanocrystals also exhibit the feature of wavelength-dependent average lifetimes (Figures S16 and S22), elongating for 1−2 orders of magnitude when the PL wavelength is red-shifted from 620 to 740 nm. With the same protocol for solution samples, we also derived TRES and EAES of films as shown in Figure 6. Apart from intramolecular torsional relaxions, intermolecular energy transfer processes could also occur in the self-organized dye layer on oxide nanocrystals, contributing to the dynamic Stokes shifts presented in Figure 6. The dynamic quenching yields (QY^D) at a variety of PL wavelengths were calculated via equation

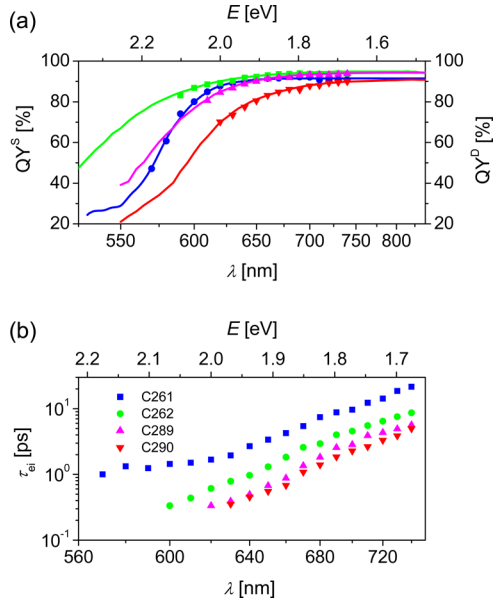

Figure 5. (a) Static PL quenching yields (QY^S, solid lines) and dynamic PL quenching yields (QY^D, symbols) of (blue) C261, (green) C262, (magenta) C289, and (red) C290. (b) Time constants of electron injection as a function of PL wavelengths.

$$QY^D(\lambda) = 1 - \frac{\bar{\tau}(T, \lambda)}{\bar{\tau}(A, \lambda)} \quad (4)$$

where $\bar{\tau}$ (T, λ) and $\bar{\tau}$ (A, λ) are the wavelength dependent PL lifetimes of dyes on titania and alumina, respectively. The values of QY^D also merged into Figure 5a are consistent with those of QY^S. The low values of QY^S and QY^D of high-energy excited states could be understood in term of the competitive transformations of them to the low-energy excited states, which are actually characteristic of high PL quenching yields.

DOI: 10.1021/acsami.6b02075
ACS Appl. Mater. Interfaces 2016, 8, 9839−9848

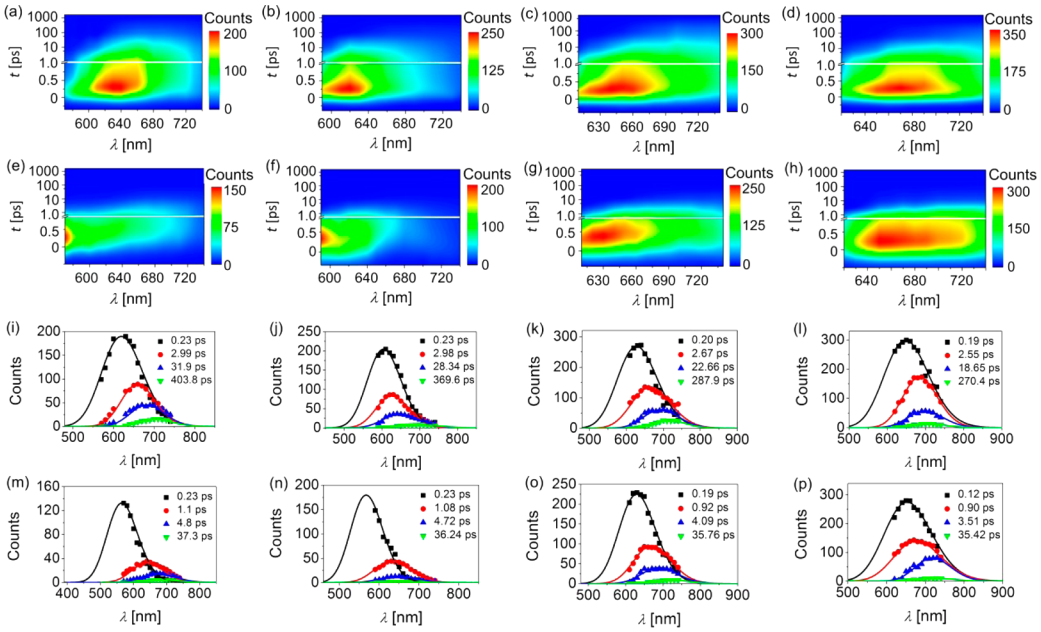

Figure 6. (a–h) Contour plots of time-resolved emission spectra (TRES) of (a) C261 grafted on alumina, (b) C262 grafted on alumina, (c) C289 grafted on alumina, (d) C290 grafted on alumina, (e) C261 grafted on titania, (f) C262 grafted on titania, (g) C289 grafted on titania, and (h) C290 grafted on titania, which were reconstructed based on the corresponding fitting curves in Figure S12–S15 and S18–S21, and static PL spectroscopies in Figure S17 and S23. (i–p) Evolution associated emission spectra (EAES) of (i) C261 grafted on alumina, (j) C262 grafted on alumina, (k) C289 grafted on alumina, (l) C290 grafted on alumina, (m) C261 grafted on titania, (n) C262 grafted on titania, (o) C289 grafted on titania, and (p) C290 grafted on titania. Time constants of spectral evolution are included. All films were immersed in the ionic liquid composite electrolyte. The solid lines were obtained via log-normal fittings.

Furthermore, we estimated the time constant of electron injection ($\overline{\tau}_{ei}$) via equation

$$\overline{\tau}_{ei}(\lambda) = \frac{1}{\frac{1}{\overline{\tau}(T,\lambda)} - \frac{1}{\overline{\tau}(A,\lambda)}} \quad (5)$$

The values of $\overline{\tau}_{ei}$ of C261, C262, C289, and C290 at the excited states emitting a variety of photons are compared in Figure 5b. For each dye over 1 order of magnitude elongation of $\overline{\tau}_{ei}$ was noted upon a attenuation of the free energy of excited state from 2.0 to 1.7 eV. Obviously, the values of $\overline{\tau}_{ei}$ are very dispersive owing to the broad energy distribution of excited states.

For excited states transmitting the same photons, we deduce that the free energy of C261 should be lower than those of the other three dyes, in consideration of the lower HOMO energy level of C261 compared to C262, C289, and C290 (Table 1). Therefore, it is very sensible to observe a larger $\overline{\tau}_{ei}$ for C261 at a given energy of PL, in terms of the driving energy of electron injection. Because the HOMO energy level (Table 1) of three BT-containing dyes are not too much different, their excited states emitting the same photons should have a similar free energy, and thus a comparable driving energy for electron injection. Thereby, the variation of $\overline{\tau}_{ei}$ in the order of C262 > C289 > C290 could be attributed to the step-by-step structural planarization, which is likely to enhance the electronic coupling of dye molecules in the excited state with titania, decrease the reorganization energy of electron injection, or both.[46]

To fabricate DSCs with an ionic liquid composite electrolyte, a bilayer porous titania film which was presintered on a fluorine-doped tin oxide (FTO) glass, were employed to adsorb dye molecules. For the electrolyte composition and manufacture details, see the Experimental Section. We recorded EQEs of DSCs made with these four DPA-PC dyes at short-circuit, under an irradiance of white light bias (10 mW cm^{-2}) and monochromatic light at the 10 nm wavelength interval. As Figure 7a shows, the broadest EQE response of C290 is firmly relevant to the narrowest optical energy gap (Figure 7b) of a translucent titania film grafted with this dye. In addition, dye C290 with EBTEBA as the electron-acceptor acquires the largest EQE peak value of 85%, even though it has the lowest LUMO energy level among the herein studied four DPA-PC dyes. This observation has suggested that the yield of electron injection at the dye/titania interface should not be reduced albeit the smallest driving energy. In stark contrast, dye C262 with the largest optical energy gap carries the lowest EQE maximum, owing to the poor light harvesting efficiencies (LHEs) in the green spectral region. It can also be noted that another BT-containing dye C289 owns an EQE height comparable to C290, and holds an onset wavelength of photocurrent in the middle of C262 and C290. The relative lower EQE maximum of C261 with respect to C289 is only partially related to the slightly weaker LHEs in the spectral region from 525 to 725 nm (Figure 7b). Actually, we suspect that its main origin could be diminished electron collection yield.

The photocurrent density–voltage (*J*-*V*) characteristics (Figure 7c) were further recorded at an irradiance of 100 mW cm^{-2}, simulated AM1.5 sunlight to evaluate the photovoltaic parameters (Table 2) of DSCs. Dye C261 exhibits a short-circuit photocurrent density (J_{SC}) of 11.98 mA cm^{-2}, a V_{OC} of 713 mV, and a fill factor (FF) of 74.0%, yielding a moderate PCE of 6.3% for ionic liquid based DSCs. However, with respect to C261 a considerably diminished J_{SC} of 8.83 mA cm^{-2} was measured for dye C262, leading to a ~22% decreased PCE of 4.9%, despite a 16 mV larger V_{OC} of 729 mV and an augmented FF of 76.1%. Moreover, compared to C261 and

DOI: 10.1021/acsami.6b02075
ACS Appl. Mater. Interfaces 2016, 8, 9839–9848

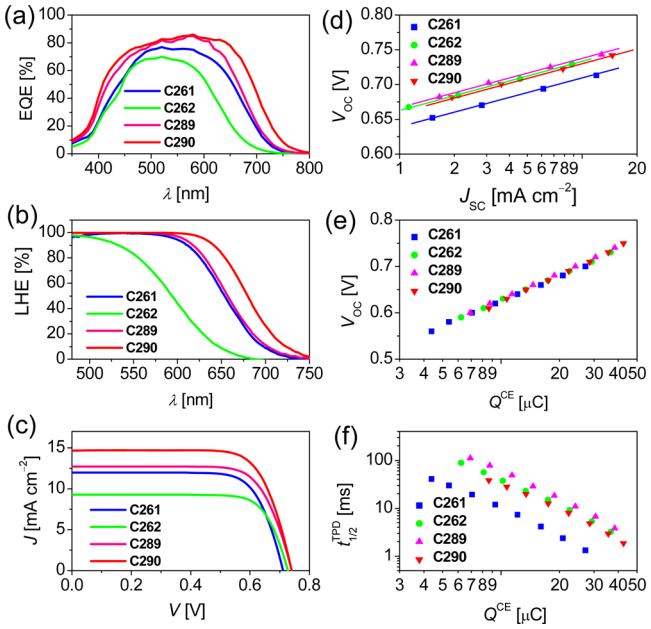

Figure 7. (a) Plots of external quantum efficiencies (EQEs) as a function of wavelengths (λ) for DSCs made with dye-grafted bilayer (4.6 + 5.0 μm thick) titania films in collaboration with an ionic liquid composite electrolyte. (b) Wavelength-dependent light-harvesting yields (LHE) of 8.0 μm thick mesoporous titania films grafted with dye molecules and also immersed in an ionic liquid composite electrolyte. (c) Current–voltage (J–V) curves measured under an irradiance of 100 mW cm^{-2} simulated AM1.5G sunlight. On top of a DSC was laminated with an antireflection film. The aperture area of our metal mask was 0.160 cm^2. (d) Open-circuit photovoltages (V_{OC}) plotted against short-circuit photocurrent densities (J_{SC}). The solid linear fittings were also included. (e) Plots of charges extracted from a dye-grafted titania film (Q^{CE}) versus V_{OC}. (f) Plots of electron half-lifetimes ($t_{1/2}^{TPD}$) as a function of Q^{CE}.

C262, dye C289 not only owns an improved J_{SC} of 12.81 mA cm^{-2} but also possesses an enhanced V_{OC} of 743 mV, affording a good PCE of 7.0%. Owing to the broadest EQE response and the largest EQE peak value, dye C290 achieves the highest J_{SC} of 14.65 mA cm^{-2} among the four DPA-PC dyes, the almost same V_{OC} of 742 mV as C289, engendering an impressive PCE of 8.0%. To understand the influence of electrolytes (a cobalt based volatile electrolyte versus an iodine based ionic liquid electrolyte) on the efficiency of DSCs, we also used a standard tris(2,2′-bipyridine)cobalt(II/III) electrolyte for device fabrication with the four DPA-PC dyes, and compiled the detailed photovoltaic parameters in Table S14. In general, each dye can display a higher PCE owing to an increase of V_{OC}.

J–V curves of DSCs made with the ionic liquid composite electrolyte were also scanned under various irradiances by employing various neutral metal meshes. We plotted V_{OC} as a logarithmic function of J_{SC} in Figure 7d and obtained four almost parallel fitting lines (blue, green, magenta, and red), showing that one order magnitude step-up of J_{SC} induces an ~68 mV increment of V_{OC}. We have also noted that at a given J_{SC}, V_{OC} augments in the order C261 ≪ C290 < C262 < C289. To unlock the interfacial energetics and kinetics underlying the variation of V_{OC},[47,48] charge extraction (CE) and transient photovoltage decay (TPD) measurements were further performed.[49,50] As shown in Figure 7e, the plots of charges (Q^{CE}) as a function of V_{OC} suggest an identical CB edge and profile of trap states under CB of titania while altering the dye molecules. Clearly, a higher V_{OC} is intimately related to more charges stored in titania. In a simplified picture, the interface diploe should be impacted by protons and deprotonated dyes on titania, formed via dissociated adsorption of neutral dye molecules. Note that a different dye may have a dissimilar dipole. In addition the loading amount and tilt angle of dye molecules will affect the overall interface dipole. Moreover, if the loading amounts of dye molecules on titania are different, the loading amounts of electrolyte additive such as lithium ions and TBP on titania will also be changed. We also conceive that the mobile ions in the liquid version of DSCs will be located in the self-assembled dye layer and thereby screen the interface dipole caused by dye molecules. In our recent experiments of using the 100 ns resolved charge extraction method to scrutinize the impact of dye molecules, we normally did not probe a significant change of the CB edge of titania if the electrolyte and titania are fixed. However, we have found that at a certain Q^{CE}, the half lifetimes ($t_{1/2}^{TPD}$) of electrons in titania are divergent and escalate in the order C261 ≪ C290 < C262 < C289 (Figure 7f), mirroring the aforementioned V_{OC} variation. Short electron lifetime of the cell with C261 could exert an unfavorable impact on electron diffusion length, resulting in poor electron collection yield as already indicated by EQE curves in Figure 7a. Resorting to visible spectrometry, dye loading amount (c_m) were further identified to be 1.6 × 10^{-8} mol cm^{-2} μm^{-1} for C261, 1.3 × 10^{-8} mol cm^{-2} μm^{-1} for C262, 2.6 × 10^{-8} mol cm^{-2} μm^{-1} for C289, and 2.8 × 10^{-8} mol cm^{-2} μm^{-1} for C290, which, however, do not present a clear relationship with $t_{1/2}^{TPD}$, owing to the critical contributions of other factors such as molecular length and packing mode.

Finally, we submitted DSCs made with the DPA-PC dyes and ionic liquid composite electrolyte to the 1000 h aging test under an irradiance of AM1.5G sunlight at 60 °C. The photovoltaic parameters after aging were collected in Table 2,

Table 2. Averaged Photovoltaic Parameters of 4 Cells Measured at an Irradiance of 100 mW cm^{-2} Simulated AM1.5G Sunlight

cell	J_{SC}^{EQE} (mA cm^{-2})[a]	J_{SC} (mA cm^{-2})	V_{OC} (mV)	FF (%)	PCE (%)
C261/fresh	12.27 ± 0.13	11.98 ± 0.10	713 ± 3	74.0 ± 0.3	6.3 ± 0.1
C261/aged	12.24 ± 0.12	11.97 ± 0.20	699 ± 3	76.5 ± 0.4	6.4 ± 0.1
C262/fresh	9.13 ± 0.18	8.83 ± 0.16	729 ± 5	76.1 ± 0.04	4.9 ± 0.1
C262/aged	8.46 ± 0.16	8.20 ± 0.12	643 ± 4	76.4 ± 0.03	4.0 ± 0.2
C289/fresh	13.58 ± 0.11	12.81 ± 0.12	743 ± 4	74.0 ± 0.05	7.0 ± 0.1
C289/aged	11.95 ± 0.10	12.02 ± 0.10	640 ± 3	75.0 ± 0.04	5.8 ± 0.2
C290/fresh	15.21 ± 0.12	14.65 ± 0.09	742 ± 3	73.6 ± 0.05	8.0 ± 0.1
C290/aged	15.31 ± 0.11	14.76 ± 0.07	667 ± 2	74.5 ± 0.03	7.4 ± 0.2

[a] J_{SC}^{EQE} was derived via wavelength integration of the product of the standard AM1.5G emission spectrum (ASTM G173-03) and the EQE curve was measured at the short-circuit.

DOI: 10.1021/acsami.6b02075
ACS Appl. Mater. Interfaces 2016, 8, 9839–9848

and more details were presented in Figure S24 of the Supporting Information. The aged cells with C261, C262, C289, and C290 retain 102, 82, 83, and 93% of their initial PCE values, respectively. It is noted that the light and thermal dual stress has induced a general drop of V_{OC}, partially stemming from the downward movement of CB edge (Figure S25). As Figure S25 shows, a remarkable decrease of $t_{1/2}^{TPD}$ of electrons in titania has been identified for cells with C262 and C289. This could be somehow relevant to the desorption of dye molecules from the surface of titania (Figure S26). Importantly, no decrease of light absorption and EQEs could be probed from Figure S26 for the efficient cell with C290, which is in good agreement of its remarkably stable J_{SC}. Our study has removed the main concern on the chemical addition of iodine to the two triple bonds in electron-acceptor EBTEBA.

3. CONCLUSIONS

To summarize, we have employed electron-acceptors EBTBA and EBTEBA in collaboration with electron-donor DPA-PC to construct two new D−A dyes, which exhibit enhanced power conversion efficiencies in comparison with the two control dyes with CA and BTBA as electron-acceptors. For the first time, we have demonstrated that triple bond containing organic compounds can also be used as sensitizers to fabricate stable solar cells with an iodine electrolyte. DFT calculations and electrochemical measurements have revealed that the new electron-acceptors BTBA, EBTBA, and EBTEBA can confer a D−A dye with FMO energy levels closer to its electron-donor and electron-acceptor than the traditional electron-acceptor CA. We have disclosed the presence of dynamic Stokes shifts for these DPA-PC dyes not only dissolved in toluene but also grafted on oxide nanocrystals, which are highly relevant to torsional relaxations of excited state. Ultrafast intramolecular and intermolecular excited state relaxations are likely to compete with electron injection, which should be attenuated in the future materials and device development in organic dye-sensitized solar cells. In addition, owing to the broad energy distribution of excited states in organic dye sensitized solar cells, the electron injection kinetics are very dispersive.

4. EXPERIMENTAL SECTION

4.1. Materials. 3α,7α-Dihyroxy-5β-cholic acid (cheno), EMITFSI, decamethylferrocene (DMFc), ferrocene (Fc), 4-*tert*-butylpyridine (TBP), lithium bis(trifluoromethanesulfonyl)imide (LiTFSI), guanidinium thiocyanate (GNCS), and sulfolane were bought from Sigma-Aldrich. Tris(dibenzylideneacetone)dipalladium ($Pd_2(dba)_3$), cesium carbonate (Cs_2CO_3), tris(1,1-dimethylethyl)phosphine ($P(t\text{-}Bu)_3$), and KOH were purchased from Alfa-Aesar. THF, toluene, dioxane, acetonitrile, ethanol, and chloroform were distilled before use. 1,3-Dimethylimidazolium iodide (DMII),[51] 1-ethyl-3-methylimidazolium iodide (EMII),[51] *N*-butylbenzimidazole (NBB),[52] 10-bromo-1-(2-hexyldecyl)-*N*,*N*-bis(4-(hexyloxy)phenyl)-1*H*-phenanthro[1,10,9,8-*cdefg*]carbazol-3-amine (**1**),[34] butyl 4-(7-ethynylbenzo[*c*][1,2,5]-thiadiazol-4-yl)benzoate,[36] and butyl 4-((7-ethynylbenzo[*c*][1,2,5]-thiadiazol-4-yl)ethynyl)benzoate,[37] C261,[34] and C262[35] were prepared according to the literature routes, respectively. The synthetic details of C289 and C290 are described as follows.

4-(7-((10-(Bis(4-(hexyloxy)phenyl)amino)-1-(2-hexyldecyl)-1H-phenanthro[1,10,9,8-cdefg]carbazol-3-yl)ethynyl)benzo[c][1,2,5]-thiadiazol-4-yl)benzoic Acid (C289). Compound **1** (936 mg, 1.00 mmol) and butyl 4-(7-ethynylbenzo[*c*][1,2,5]thiadiazol-4-yl)benzoate (403 mg, 1.20 mmol) were disolved in dioxane (16 mL) in a 50 cc two-necked round-bottom flask. Then $Pd_2(dba)_3$ (33 mg, 0.04 mmol), $P(t\text{-}Bu)_3$ (12 mg, 0.06 mmol), and Cs_2CO_3 (391 mg, 1.20 mmol) were added under the protection of argon flow. The resulting mixture was stirred at reflux for 5 h and terminated by adding water. Afterward, chloroform was added to extract the mixture for three times. The organic phase was dried over anhydrous magnesium sulfate and concentrated under reduced pressure. Then the residue was purified by column chromatography with the mixed eluent (toluene/petroleum ether 60−90 °C, 2/3, v/v) to obtain the desired dye precursor butyl ester. Subsequently, the butyl ester compound and KOH (493 mg, 8.80 mmol) were dissolved in a mixture solvent of THF and H_2O (11 mL, 1/3, v/v) in a 50 cc three-necked, round-bottom flask. Then, the resulting mixture was stirred at reflux overnight and extracted two times with dichloromethane before the organic phase was combined and acidified with 0.2 M phosphoric acid aqueous solution. The organic phase was dried over anhydrous magnesium sulfate and concentrated under reduced pressure. The residue was purified by column chromatography with the mixed eluent (methanol/chloroform, 1/15, v/v) to get a black solid of C289 (942 mg, 83% yield). ^{1}H NMR (400 MHz, THF-d_8) δ: 8.92 (d, J = 8.2 Hz, 1H), 8.79 (d, J = 7.6 Hz, 1H), 8.72 (d, J = 7.6 Hz, 1H), 8.29 (s, 1H), 8.23 (d, J = 8.4 Hz, 2H), 8.19 (d, J = 8.4 Hz, 2H), 8.07 (d, J = 7.4 Hz, 1H), 8.03−7.97 (m, 3H), 7.68−7.63 (m, 2H), 7.04 (d, J = 8.9 Hz, 4H), 6.77 (d, J = 8.9 Hz, 4H), 4.61 (d, J = 7.1 Hz, 2H), 3.90 (t, J = 6.3 Hz, 4H), 2.08−2.03 (m, 1H), 1.49−1.46 (m, 4H), 1.36−1.34 (m, 12H), 1.29 (br, 6H), 1.20−1.18 (m, 10H), 0.93−0.90 (m, 9H), 0.83−0.79 (m, 6H). ^{13}C NMR (100 MHz, THF-d_8) δ: 167.45, 159.92, 156.48, 153.94, 141.88, 139.71, 134.83, 134.65, 133.18, 132.37, 131.98, 131.56, 131.35, 131.09, 130.53, 129.87, 129.11, 128.90, 126.07, 125.48, 125.33, 124.93, 124.74, 122.09, 121.92, 119.07, 118.86, 118.45, 116.96, 116.37, 115.15, 114.77, 98.55, 90.80, 71.49, 50.44, 40.60, 39.13, 36.16, 32.85, 32.73, 32.50, 32.40, 31.03, 30.84, 30.68, 30.57, 30.40, 30.29, 30.18, 27.96, 27.82, 27.19, 26.37, 23.55, 23.43, 14.45, 14.38. HR-MS (MALDI-TOF) m/z calcd for ($C_{75}H_{82}N_4O_4S$): 1134.60568. Found: 1134.60579. Anal. calcd for $C_{75}H_{82}N_4O_4S$: C, 79.33%; H, 7.28%; N, 4.93%. Found: C, 79.30%; H, 7.31%; N, 4.92%.

4.1.2. 4-((7-((10-(Bis(4-(hexyloxy)phenyl)amino)-1-(2-hexyldecyl)-1H-phenanthro[1,10,9,8-cdefg]carbazol-3-yl)ethynyl)benzo[c]-[1,2,5]thiadiazol-4-yl)ethynyl)benzoic Acid (C290). Compound **1** (941 mg, 1.01 mmol) and butyl 4-((7-ethynylbenzo[*c*][1,2,5]-thiadiazol-4-yl)ethynyl)benzoate (432 mg, 1.20 mmol) were disolved in dioxane (16 mL) in a 50 cc two-necked round-bottom flask. After that, $Pd_2(dba)_3$ (33 mg, 0.04 mmol), $P(t\text{-}Bu)_3$ (12 mg, 0.06 mmol), and Cs_2CO_3 (391 mg, 1.20 mmol) were added under the protection of argon flow. The resulting mixture was stirred at reflux for 5 h and terminated by water. Then chloroform was added to extract the mixture for three times. The organic phase was dried over anhydrous magnesium sulfate and concentrated under reduced pressure. Then the residue was purified by column chromatography with the mixed eluent (toluene/petroleum ether 60−90 °C, 3/4, v/v) to yield the dye precursor butyl ester. Whereafter, the butyl ester compound and KOH (493 mg, 8.80 mmol) were dissolved in a mixture solvent of THF and H_2O (12 mL, 1/3, v/v) in a 50 cc. three-necked, round-bottom flask. Then, the resulting mixture was stirred at reflux overnight and extracted two times with dichloromethane before the organic phase was combined and acidified with 0.2 M phosphoric acid aqueous solution. The organic phase was dried over anhydrous magnesium sulfate and concentrated under reduced pressure. Then, the residue was purified by column chromatography with the mixed eluent (methanol/chloroform, 1/10, v/v) to get a black powder of C290 (880 mg, 76% yield). ^{1}H NMR (400 MHz, THF-d_8) δ: 8.87 (d, J = 7.8 Hz, 1H), 8.77 (d, J = 7.2 Hz, 1H), 8.70 (d, J = 7.3 Hz, 1H), 8.26 (s, 1H), 8.09 (d, J = 7.2 Hz, 2H), 8.03−7.93 (m, 4H), 7.75 (d, J = 7.2 Hz, 2H), 7.67−7.63 (m, 2H), 7.05 (d, J = 7.4 Hz, 4H), 6.78 (d, J = 7.4 Hz, 4H), 4.58 (br, 2H), 3.90−3.89 (m, 4H), 2.07−2.03 (m, 1H), 1.47 (br, 4H), 1.35 (br, 10H), 1.29 (br, 8H), 1.17 (br, 10H), 0.91 (br, 9H), 0.80 (br, 6H). ^{13}C NMR (100 MHz, THF-d_8) δ: 167.20, 155.71, 155.63, 145.61, 144.16, 135.64, 133.92, 132.61, 132.31, 132.14, 131.51, 130.80, 128.51, 128.12, 126.53, 126.49, 125.62, 125.18, 124.90, 124.62, 122.58, 122.25, 119.72, 119.62, 119.42, 116.87, 116.01, 115.79, 114.91, 100.25, 97.03, 91.07, 89.17, 68.92, 50.63, 41.00, 36.36, 32.99, 32.88, 32.77, 31.03, 30.79, 30.73, 30.59, 30.54, 30.43, 30.39, 28.22, 27.50, 26.92, 23.69, 23.65, 14.60, 14.55. HR-MS (MALDI-TOF) m/z calcd for

DOI: 10.1021/acsami.6b02075
ACS Appl. Mater. Interfaces 2016, 8, 9839−9848

($C_{77}H_{82}N_4O_4S$): 1158.60568. Found: 1158.60548. Anal. calcd for $C_{77}H_{82}N_4O_4S$: C, 79.76%; H, 7.13%; N, 4.83%. Found: C, 79.72%; H, 7.15%; N, 4.86%.

4.2. Theoretical Calculations. All the calculations were performed with the Gaussian 09 suite of programs and the 6-311G(d,p) basis set was selected for all of the atoms. The solvent effects was simulated by utilizing the conductor-like polarized continuum model (C-PCM).[53] The popular B3LYP exchange-correlation functional was employed for optimization of the ground-state geometries.[54] For calculation of the vertical electron transitions and optimizations of excited-state geometries, the TD-MPW1K hybrid functional including 42% of Hartree−Fock exchange was used.[55,56]

4.3. Cell Fabrication and Measurements. In this work, a 4.2 + 5.0 μm thick double titania film deposited on FTO glass (NSG, Solar) was used as the photoanode of DSCs. The details on film preparation were outlined in a previous study.[57] A titania film was further dye-loaded by immersing it into a dye solution for 12 h. The dye solution was made by dissolving 150 μM of dye and 30 mM of cheno in a chloroform-ethanol mixture (v/v, 1/9 for C261; 3/7 for C262, C289, and C290). The dye-grafted titania film was assembled with a gold coated FTO electrode by employing an O-ring (Surlyn, 25 μm thick) to fabricate a thin-layer electrochemical cell. The iodine-based ionic liquid composite electrolyte is composed of DMII, EMIII, sulfolane, iodine, NBB, and GNCS at a molar ratio of 12/12/16/1.67/3.33/0.67. Detailed description on EQE, $J-V$, charge extraction and photovoltage decay measurements could be found in our previous publications.[58,59]

4.4. PL Measurements. Being similar to the procedure for DSC manufacture, the cell for spectroscopic measurements was made by splicing a dye-adsorbed mesoporous oxide film with a bare FTO. The ionic liquid composite electrolyte was employed to fill the internal space. An ICCD camera detector in combination with a cw laser excitation at 490 nm was used to record steady PL spectra. The details on femtosecond fluorescence up-conversion measurements were depicted in our previous work.[60] In brief, the output of 130 fs pulses at 800 nm from a regenerative amplifier (Spitfire, Spectra Physics) was split into two parts by using a 9/1 beam splitting prism. The larger portion was sent to an optical parametric amplifier (TOPAS-C, Light Conversion) to afford a excitation light at 490 nm. The minor portion was directed to a 0.3 mm thick BBO crystal to overlap with the photons emitted from a rotating sample and yield a sum frequency light. Pump intensity dependent kinetics were slipped in our measurements. TRESs of the toluene solutions were also recorded on a LifeSpec-II fluorescence spectrometer, operating in a time-correlated single photon counting mode. Resorting to the free Glotaran software, we carried out the Global analysis for PL traces.[39] To get a satisfactory global fitting, at least four time constants were requested. Then, every kinetic trace was fitted to obtain the corresponding amplitudes by using the four time constants in the Surface Xplorer software (version 2.3).

4.5. Voltammetric and Electronic Absorption Measurements. We employed a CHI660C electrochemical workstation and a three-electrode electrolytic cell to measure CVs of dyes dissolved in THF. To obtain well-defined CVs, a slow potential scan rate of 5 mV s^{-1} was used, and the iR drop was compensate. An Agilent G1103A spectrometer equipped with a silicon diode array detector was used to record electronic absorption spectroscopies.

■ ASSOCIATED CONTENT

Supporting Information

The Supporting Information is available free of charge on the ACS Publications website at DOI: 10.1021/acsami.6b02075.

Additional data on theoretical calculations, spectroscopies, and photovoltaic parameters. (PDF)

■ AUTHOR INFORMATION

Corresponding Author

* E-mail: pw2015@zju.edu.cn or peng.wang@ciac.ac.cn. Telephone: 0086-571-88273217.

Notes

The authors declare no competing financial interest.

■ ACKNOWLEDGMENTS

This work was financed by the National 973 Program (2015CB932204) and the National Science Foundation of China (No. 91233206 and No. 51125015).

■ REFERENCES

(1) O'Regan, B.; Grätzel, M. A Low-Cost, High-Efficiency Solar Cell Based on Dye-Sensitized Colloidal TiO_2 Films. *Nature* **1991**, *353*, 737−740.

(2) Yang, W. S.; Noh, J. H.; Jeon, N. J.; Kim, Y. C.; Ryu, S.; Seo, J.; Seok, S. I. High-Performance Photovoltaic Perovskite Layers Fabricated through Intramolecular Exchange. *Science* **2015**, *348*, 1234−1237.

(3) Kakiage, K.; Aoyama, Y.; Yano, T.; Oya, K.; Fujisawa, J.; Hanaya, M. Highly-Efficient Dye-Sensitized Solar Cells with Collaborative Sensitization by Silyl-Anchor and Carboxy-Anchor Dyes. *Chem. Commun.* **2015**, *51*, 15894−15897.

(4) Mishra, A.; Fischer, M. K. R.; Bäuerle, P. Metal-Free Organic Dyes for Dye-Sensitized Solar Cells: from Structure: Property Relationships to Design Rules. *Angew. Chem., Int. Ed.* **2009**, *48*, 2474−2499.

(5) Imahori, H.; Umeyama, T.; Ito, S. Large π-Aromatic Molecules as Potential Sensitizers for Highly Efficient Dye-Sensitized Solar Cells. *Acc. Chem. Res.* **2009**, *42*, 1809−1818.

(6) Clifford, J. N.; Martínez-Ferrero, E.; Viterisi, A.; Palomares, E. Sensitizer Molecular Structure-Device Efficiency Relationship in Dye Sensitized Solar Cells. *Chem. Soc. Rev.* **2011**, *40*, 1635−1646.

(7) Li, C.; Wonneberger, H. Perylene Imides for Organic Photovoltaics: Yesterday, Today, and Tomorrow. *Adv. Mater.* **2012**, *24*, 613−636.

(8) Yen, Y.-S.; Chou, H.-H.; Chen, Y.-C.; Hsu, C.-Y.; Lin, J. T. Recent Developments in Molecule-Based Organic Materials for Dye-Sensitized Solar Cells. *J. Mater. Chem.* **2012**, *22*, 8734−8747.

(9) Wu, Y.; Zhu, W. Organic Sensitizers from D-π-A to D−A-π-A: Effect of the Internal Electron-Withdrawing Units on Molecular Absorption, Energy Levels and Photovoltaic Performances. *Chem. Soc. Rev.* **2013**, *42*, 2039−2058.

(10) Liang, M.; Chen, J. Arylamine Organic Dyes for Dye-Sensitized Solar Cells. *Chem. Soc. Rev.* **2013**, *42*, 3453−3488.

(11) Nusbaumer, H.; Moser, J.-E.; Zakeeruddin, S. M.; Nazeeruddin, M. K.; Grätzel, M. $Co^{II}(dbbip)_2^{2+}$ Complex Rivals Tri-iodide/Iodide Redox Mediator in Dye-Sensitized Solar Cells. *J. Phys. Chem. B* **2001**, *105*, 10461−10464.

(12) Hattori, S.; Wada, Y.; Yanagida, S.; Fukuzumi, S. Blue Copper Model Complexes with Distorted Tetragonal Geometry Acting as Effective Electron-Transfer Mediators in Dye-Sensitized Solar Cells. *J. Am. Chem. Soc.* **2005**, *127*, 9648−9654.

(13) Feldt, S. M.; Gibson, E. A.; Gabrielsson, E.; Sun, L.; Boschloo, G.; Hagfeldt, A. Design of Organic Dyes and Cobalt Polypyridine Redox Mediators for High-Efficiency Dye-Sensitized Solar Cells. *J. Am. Chem. Soc.* **2010**, *132*, 16714−16724.

(14) Daeneke, T.; Kwon, T.-H.; Holmes, A. B.; Duffy, N. W.; Bach, U.; Spiccia, L. High-Efficiency Dye-Sensitized Solar Cells with Ferrocene-based Electrolytes. *Nat. Chem.* **2011**, *3*, 211−215.

(15) Bai, Y.; Zhang, J.; Zhou, D.; Wang, Y.; Zhang, M.; Wang, P. Engineering Organic Sensitizers for Iodine-Free Dye-Sensitized Solar Cells: Red-Shifted Current Response Concomitant with Attenuated Charge Recombiantion. *J. Am. Chem. Soc.* **2011**, *133*, 11442−11445.

(16) Yella, A.; Lee, H.-W.; Tsao, H. N.; Yi, C.; Chandiran, A. K.; Nazeeruddin, M. K.; Diau, E. W.-G.; Yeh, C.-Y.; Zakeeruddin, S. M.; Grätzel, M. Porphyrin-Sensitized Solar Cells with Cobalt(II/III)−Based Redox Electrolyte Exceed 12% Efficiency. *Science* **2011**, *334*, 629−634.

(17) Mathew, S.; Yella, A.; Gao, P.; Humphry-Baker, R.; Curchod, B. F. E.; Ashari-Astani, N.; Tavernelli, I.; Rothlisberger, U.; Nazeeruddin,

DOI: 10.1021/acsami.6b02075
ACS Appl. Mater. Interfaces 2016, 8, 9839−9848

M. K.; Grätzel, M. Dye-Sensitized Solar Cells with 13% Efficiency Achieved Through the Molecular Engineering of Porphyrin Sensitizers. *Nat. Chem.* **2014**, *6*, 242−247.
(18) Yao, Z.; Wu, H.; Li, Y.; Wang, J.; Zhang, J.; Zhang, M.; Guo, Y.; Wang, P. Dithienopicenocarbazole as the Kernal Module of Low-Energy-Gap Organic Dyes for Efficient Conversion of Sunlight to Electricity. *Energy Environ. Sci.* **2015**, *8*, 3192−3197.
(19) Wang, P.; Zakeeruddin, S. M.; Humphry-Baker, R.; Moser, J. E.; Grätzel, M. Molecualr-Scale Interface Engineering of TiO_2 Nanocrystals: Improving the Efficiency and Stability of Dye-Sensitized Solar Cells. *Adv. Mater.* **2003**, *15*, 2101−2104.
(20) Zhang, M.; Zhang, J.; Fan, Y.; Yang, L.; Wang, Y.; Li, R.; Wang, P. Judicious Selection of a Pinhole Defect Filler to Generally Enhance the Performance of Organic Dye-Sensitized Solar Cells. *Energy Environ. Sci.* **2013**, *6*, 2939−2943.
(21) Kakiage, K.; Aoyama, Y.; Yano, T.; Otsuka, T.; Kyomen, T.; Unno, M.; Hanaya, M. An Achievement of Over 12% Efficiency in an Organic Dye-Sensitized Solar cell. *Chem. Commun.* **2014**, *50*, 6379−6381.
(22) Bai, Y.; Mora-Seró, I.; De Angelis, F.; Bisquert, J.; Wang, P. Titanium Dioxide Nanomaterials for Photovolatic Applications. *Chem. Rev.* **2014**, *114*, 10095−10130.
(23) Li, J.-Y.; Chen, C.-Y.; Lee, C.-P.; Chen, S.-C.; Lin, T.-H.; Tsai, H.-H.; Ho, K.-C.; Wu, C.-G. Unsymmetrical Squaraines Incorporating the Thiophene Unit for Panchromatic Dye-Sensitized Solar Cells. *Org. Lett.* **2010**, *12*, 5454−5457.
(24) Funabiki, K.; Mase, H.; Hibino, A.; Tanaka, N.; Mizuhata, N.; Sakuragi, Y.; Nakashima, A.; Yoshida, T.; Kubota, Y.; Matsui, M. Synthesis of a Novel Heptamethine-Cyanine Dye for Use in Near-Infrared Active Dye-Sensitized Solar Cells with Porous Zinc Oxide Prepared at Low Temperature. *Energy Environ. Sci.* **2011**, *4*, 2186−2192.
(25) Maeda, T.; Arikawa, S.; Nakao, H.; Yagi, S.; Nakazumi, H. Linearly π-Extended Squaraine Dyes Enable the Spectral Response of Dye-Sensitized Solar Cells in the NIR Region Over 800 nm. *New J. Chem.* **2013**, *37*, 701−708.
(26) Chen, C.; Yang, X.; Cheng, M.; Zhang, F.; Zhao, J.; Sun, L. Efficient Panchromatic Organic Sensitizers with Dihydrothiazole Derivative as π-Bridge for Dye-Sensitized Solar Cells. *ACS Appl. Mater. Interfaces* **2013**, *5*, 10960−10965.
(27) Ardo, S.; Meyer, G. J. Photodriven Heterogeneous Charge Transfer with Transition-Metal Compounds Anchored to TiO_2 Semiconductor Surfaces. *Chem. Soc. Rev.* **2009**, *38*, 115−164.
(28) Listorti, A.; O'Regan, B.; Durrant, J. R. Electron Transfer Dynamics in Dye-Sensitized Solar Cells. *Chem. Mater.* **2011**, *23*, 3381−3399.
(29) Griffith, M. J.; Sunahara, K.; Wagner, P.; Wagner, K.; Wallace, G. G.; Officer, D. L.; Furube, A.; Katoh, R.; Mori, S.; Mozer, A. J. Porphyrins for Dye-Sensitized Solar Cells: New Insights into Efficiency-Determining Electron Transfer Steps. *Chem. Commun.* **2012**, *48*, 4145−4162.
(30) Englman, R.; Jortner, J. Energy Gap Law for Radiationless Transitions in Large Molecules. *Mol. Phys.* **1970**, *18*, 145−164.
(31) Luo, J.; Xu, M.; Li, R.; Huang, K.-W.; Jiang, C.; Qi, Q.; Zeng, W.; Zhang, J.; Chi, C.; Wang, P.; Wu, J. *N*-Annulated Perylene as an Efficient Electron Donor for Porphyrin-Based Dyes: Enhanced Light-Harvesting Ability and High-Efficiency Co(II/III)-Based Dye-Sensitized Solar Cells. *J. Am. Chem. Soc.* **2014**, *136*, 265−272.
(32) Li, R.; Liu, J.; Cai, N.; Zhang, M.; Wang, P. Synchronously Reduced Surface States, Charge Recombination, and Light Absorption Length for High-Performance Organic Dye-Sensitized Solar Cells. *J. Phys. Chem. B* **2010**, *114*, 4461−4464.
(33) Zhang, M.; Wang, Y.; Xu, M.; Ma, W.; Li, R.; Wang, P. Design of High-Efficiency Organic Dyes for Titania Solar Cells Based on the Chromophoric Core of Cyclopentadithiophene-Benzothiadiazole. *Energy Environ. Sci.* **2013**, *6*, 2944−2949.
(34) Yao, Z.; Yan, C.; Zhang, M.; Li, R.; Cai, Y.; Wang, P. *N*-Annulated Perylene as a Coplanar π-Linker Alternative to Benzene as a Low Energy-Gap, Metal-Free Dye in Sensitized Solar Cells. *Adv. Energy Mater.* **2014**, *4*, 1400244.
(35) Zhang, M.; Yao, Z.; Yan, C.; Cai, Y.; Ren, Y.; Zhang, J.; Wang, P. Unraveling the Pivotal Impacts of Electron-Acceptor on Light Absorption and Carrier Photogeneration in Perylene Dye Sensitized Solar Cells. *ACS Photonics* **2014**, *1*, 710−717.
(36) Yang, L.; Ren, Y.; Yao, Z.; Yan, C.; Ma, W.; Wang, P. Electron-Acceptor-Dependent Light Absorption and Charge-Transfer Dynamics in *N*-Annulated Perylene Dye-Sensitized Solar Cells. *J. Phys. Chem. C* **2015**, *119*, 980−988.
(37) Ren, Y.; Li, Y.; Chen, S.; Liu, J.; Zhang, J.; Wang, P. Improving the Performance of Dye-Sensitized Solar Cells with Electron-Donor and Electron-Acceptor Characteristic of Planar Electronic Skeletons. *Energy Environ. Sci.* **2016**, *9*, DOI: 10.1039/C5EE03309H.
(38) Adamo, C.; Jacquemin, D. The Calculations of Excited-State Properties with Time-Dependent Density Functional Theory. *Chem. Soc. Rev.* **2013**, *42*, 845−856.
(39) Snellenburg, J. J.; Laptenok, S. P.; Seger, R.; Mullen, K. M.; van Stokkum, I. H. M. Glotaran: A Java-Based Graphical User Interface for the R Package TIMP. *J. Stat. Softw.* **2012**, *49*, 1−22.
(40) Lanzani, G.; Nisoli, M.; De Silvestri, S.; Tubino, R. Femtosecond Vibrational and Torsional Energy Redistribution in Photoexcited Oligothiophenes. *Chem. Phys. Lett.* **1996**, *251*, 339−345.
(41) Kukura, P.; McCamant, D. W.; Yoon, S.; Wandschneider, D. B.; Mathies, R. A. Structural Observation of the Primary Isomerization in Vision with Femtosecond-Stimulated Raman. *Science* **2005**, *310*, 1006−1009.
(42) Westenhoff, S.; Beenken, W. J. D.; Friend, R. H.; Greenham, N. C.; Yartsev, A.; Sundström, V. Anomalous Energy Transfer Dynamics due to Torsional Relaxation in a Conjugated Polymer. *Phys. Rev. Lett.* **2006**, *97*, 166804.
(43) Parkinson, P.; Muller, C.; Stingelin, N.; Johnston, M. B.; Herz, L. M. Role of Ultrafast Torsional Relaxation in the Emission from Polythiophene Aggregates. *J. Phys. Chem. Lett.* **2010**, *1*, 2788−2792.
(44) Clark, J.; Nelson, T.; Tretiak, S.; Cirmi, G.; Lanzani, G. Femtosecond Torsional Relaxation. *Nat. Phys.* **2012**, *8*, 225−231.
(45) Yu, W.; Zhou, J.; Bragg, A. E. Exciton Conformational Dynamics of Poly(3-hexylthiophene) (P3HT) in Solution from Time-Resolved Resonant-Raman Spectroscopy. *J. Phys. Chem. Lett.* **2012**, *3*, 1321−1328.
(46) Marcus, R. A.; Sutin, N. Electron Transfers in Chemistry and Biology. *Biochim. Biophys. Acta, Rev. Bioenerg.* **1985**, *811*, 265−322.
(47) Bisquert, J. Chemical Capacitance of Nanostructured Semiconductors: Its Origin and Significance for Nanocomposite Solar Cells. *Phys. Chem. Chem. Phys.* **2003**, *5*, 5360−5364.
(48) O'Regan, B. C.; Durrant, J. R. Kinetic and Energetic Paradigms for Dye-Sensitized Solar Cells: Moving from the Ideal to the Real. *Acc. Chem. Res.* **2009**, *42*, 1799−1808.
(49) Duffy, N. W.; Peter, L. M.; Rajapakse, R. M. G.; Wijayantha, K. G. U. A Novel Charge Extraction Method for the Study of Electron Transport and Interfacial Transfer in Dye Sensitised Nanocrystalline Solar Cells. *Electrochem. Commun.* **2000**, *2*, 658−662.
(50) O'Regan, B. C.; Bakker, K.; Kroeze, J.; Smit, H.; Sommeling, P.; Durrant, J. R. Measuring Charge Transport from Transient Photovoltage Rise Times. A New Tool to Investigate Electron Transport in Nanoparticle Films. *J. Phys. Chem. B* **2006**, *110*, 17155−17160.
(51) Cao, Y.; Zhang, J.; Bai, Y.; Li, R.; Zakeeruddin, S. M.; Grätzel, M.; Wang, P. Dye-Sensitized Solar Cells with Solvent-Free Ionic Liquid Electrolytes. *J. Phys. Chem. C* **2008**, *112*, 13775−13781.
(52) Pilarski, B. A New Method for *N*-Alkylation of Imidazoles and Benzimidazoles. *Liebigs Ann. Chem.* **1983**, *1983*, 1078−1080.
(53) Cossi, M.; Rega, N.; Scalmani, G.; Barone, V. Energies, Structures, and Electronic Properties of Molecules in Solution with the C-PCM Solvation Model. *J. Comput. Chem.* **2003**, *24*, 669−681.
(54) Becke, A. D. A New Mixing of Hartree-Fock and Local Density-Functional Theories. *J. Chem. Phys.* **1993**, *98*, 1372−1377.
(55) Lynch, B. J.; Fast, P. L.; Harris, M.; Truhlar, D. G. Adiabatic Connection for Kinetics. *J. Phys. Chem. A* **2000**, *104*, 4811−4815.

DOI: 10.1021/acsami.6b02075
ACS Appl. Mater. Interfaces 2016, 8, 9839−9848

(56) Pastore, M.; Mosconi, E.; De Angelis, F.; Grätzel, M. A Computational Investigation of Organic Dyes for Dye-Sensitized Solar Cells: Benchmark, Strategies, and Open Issues. *J. Phys. Chem. C* **2010**, *114*, 7205−7212.
(57) Wang, P.; Zakeeruddin, S. M.; Comte, P.; Charvet, R.; Humphry-Baker, R.; Grätzel, M. Enhance the Performance of Dye-Sensitized Solar Cells by Co-grafting Amphiphilic Sensitizer and Hexadecylmalonic Acid on TiO_2 Nanocrystals. *J. Phys. Chem. B* **2003**, *107*, 14336−14341.
(58) Liu, J.; Li, R.; Si, X.; Zhou, D.; Shi, Y.; Wang, Y.; Jing, X.; Wang, P. Oligothiophene Dye-Sensitized Solar Cells. *Energy Environ. Sci.* **2010**, *3*, 1924−1928.
(59) Cai, N.; Wang, Y.; Xu, M.; Fan, Y.; Li, R.; Zhang, M.; Wang, P. Engineering of Push-Pull Thiophene Dyes to Enhance Light Absorption and Modulate Charge Recombination in Mesoscopic Solar Cells. *Adv. Funct. Mater.* **2013**, *23*, 1846−1854.
(60) Zhang, J.; Yao, Z.; Cai, Y.; Yang, L.; Xu, M.; Li, R.; Zhang, M.; Dong, X.; Wang, P. Conjugated Linker Correlated Energetics and Kinetics in Dithienopyrrole Dye-Sensitized Solar Cells. *Energy Environ. Sci.* **2013**, *6*, 1604−1614.

DOI: 10.1021/acsami.6b02075
ACS Appl. Mater. Interfaces 2016, 8, 9839−9848